

LOTUS SEEDPOD-BASED CARBON QUANTUM DOTS: PREPARATION, CHARACTERIZATION AND APPLICATION FOR Fe(III) DETECTION

KVANTNE PIKE OGLJIKA V OBLIKI STROKA LOTUSOVIH SEMEN: PRIPRAVA, KARAKTERIZACIJA IN UPORABA ZA DETEKCIJO Fe(III)

Zhouling Xie¹, Jianfa Sun², Zeijun Zhou³, Shibin Xia^{1*}

¹School of Resources and Environmental Engineering, Wuhan University of Technology, no. 171 Luoshi Street, Hongshan District, Wuhan 430070, China

²Key Laboratory of Arable Land Conservation (Middle and Lower Reaches of Yangtze River), Ministry of Agriculture/College of Resources and Environmental Sciences, Huazhong Agricultural University, Wuhan 430070, China

³China Petroleum & Chemical Corporation Jiangnan Oilfield Branch No. 1 Gas Production Plant, Chongqing 400000, China

Prejem rokopisa – received: 2020-08-13; sprejem za objavo – accepted for publication: 2020-10-05

doi:10.17222/mit.2020.160

Lotus seedpod (LS) was employed as a carbon source for the synthesis of carbon quantum dots (CQDs) using an economical and facile hydrothermal synthesis method. LS-CQDs were characterized with different techniques, including TEM, FTIR, PL, XRD, XPS, Raman spectroscopy and Uv-vis. The average particle size of LS-CQDs was found to be 2.1 ± 0.17 nm. The properties of the excitation-dependent photoluminescence of LS-CQDs were determined, and the quantum yield was calculated to be 1.9 %. The quenching effect of LS-CQDs on Fe(III) ions was also investigated. The normalized linear relationship between the increasing Fe(III) ion concentration and the fluorescence-emission intensities of LS-CQDs was established. Furthermore, the quenching mechanism for the reaction between Fe(III) ions and LS-CQDs was elucidated.

Keywords: lotus seedpod, carbon quantum dots, Fe(III) determination

Avtorji so uporabili strok lotusovih semen (LS) kot izvor za sintezo kvantnih pik ogljika (CQD) z uporabo ekonomične in enostavne metode hidrotermalne sinteze. LS-CQDs so okarakterizirali z različnimi tehnikami, vključno s TEM, FTIR, PL, XRD, XPS, Ramanovo spektralno UV-vis analizo. Izmerjena povprečna velikost delcev LS-CQDs je bila 2.1 ± 0.17 nm. Določili so lastnosti povzročeno odvisne fotoluminescence LS-CQDs in izračunani kvantni doprinos je bil 1,9 %. Raziskali so tudi kalilni efekt LS-CQDs na Fe(III). Določili so normalizirano linearno zvezo med naraščanjem koncentracije Fe(III) in intenziteti emisije fluorescence LS-CQDs. Nadalje so avtorji pojasnili še kalilni mehanizem reakcije med Fe(III) ioni in LS-CQDs.

Ključne besede: strok lotusovih semen, kvantne pike ogljika, določevanje Fe(III)

1 INTRODUCTION

Iron, especially Fe(III) ions, is one of the most basic, richest and essential metal elements in an organism, which participates in the formation of various enzymes and proteins as well as regulating many chemical reactions in living organisms.^{1,2} Insufficient or excessive Fe(III) in the human body can disrupt the metabolic activity and affect physical health, leading to the development of chronic diseases such as anemia, liver and kidney damage and heart failure.^{3,4} Besides, an Fe(III) ion contamination has become an increasingly severe environmental problem, attracting much attention in recent year.⁵ Therefore, the research on the Fe(III) detection is of great importance to both the environment and human health.

At present, the methods used for detecting Fe(III) include spectrophotometry, atomic spectroscopy, the electrochemical method and mass spectrometry.⁶⁻¹¹ These an-

alytical methods usually have a broad detection range, high sensitivity and excellent repeatability. However, there are also shortcomings such as a long detection time, cumbersome sample-preparation process, complicated operation, possible interference with another ion and expensive equipment. Thus, it is necessary to design a simple, fast and accurate method for the Fe(III) detection. In comparison with the other methods, the fluorescent-probe method is highly sensitive, relatively simple and more rapid, exhibiting fewer background signals and spanning over a wider linear dynamic range. It has become an important analytical method for the determination of metal ions.¹²⁻¹⁷ As a fluorescent probe, carbon quantum dot (CQD) has received considerable attention due to its advantages including a facile synthesis, and cost efficiency and adjustable fluorescence emission.¹⁸

A lotus seedpod (LS) is the receptacle surface of a lotus with many honeycomb holes. LS is usually treated as a waste and low-calorific fuel, but it is also used as food or a medicinal substance.¹⁹ Previous studies showed that LSs can be used as adsorbents or functional materials

*Corresponding author's e-mail:
xiashibin@126.com (Shibin Xia)

due to their high specific surface area after pyrolysis activation.^{20,21} Hence, there is a great potential for LSs to be applied in the development of novel CQDs. Compared with the other carbon sources, lotus seedpod exhibits obvious advantages including a low cost and an easy access.

In this study, LS was employed as a carbon source for synthesizing CQDs (hereinafter referred to as LS-CQDs) via the hydrothermal-synthesis method. The synthesized LS-CQDs were characterized with transmission electron microscopy (TEM), Raman spectroscopy, X-ray diffraction (XRD), X-ray photoelectron spectroscopy (XPS) and Fourier transform infrared (FTIR). The effect of the quenching mechanism of Fe(III) on the photoluminescence (PL) intensity of LS-CQDs was also elucidated.

2 EXPERIMENTAL PART

2.1 Instruments and materials

A homegrown mature lotus seedpod was purchased at a local supermarket (Wuhan, Hubei, in the summer). The reagents used in this study included quinoline sulfate, calcium chloride, ferric chloride, chromium tri-chloride, sodium chloride, aluminum chloride, potassium chloride, magnesium chloride and zinc chloride. All the reagents were of analytical grade and were used as received. Distilled water was used to prepare the Fe(III) ion solution.

TEM measurement was carried out using a high-resolution JEM-2100F transmission electron microscope. Raman spectral measurement was conducted using an InVia Raman spectrometer. The PL intensity was measured with spectrofluorometric detection (Sigma-Aldrich). The particle-size distribution of CQDs was analyzed using dynamic laser-light scattering. Spectrophotometric measurement was performed using a UNICOWFUV-2 UV-Vis spectrometer. XRD patterns were assessed with a D8 Advance X-ray diffractometer. XPS measurement was conducted using an ESCALAB Xi+ X-ray photoelectron spectrum analyzer. FTIR assessment was carried out using a Nexus FTIR spectrometer. Other instruments such as an electronic balance (BS223S), drying box (DGG-9123A), PTFE-lined hydrothermal synthesis reactor (LSRP-25), centrifuge (TG16-II) and lyophilizer (JL-D10N-50C) were also used in this study.

2.2 Preparation of a dried LS

Lotus seeds were removed from a fresh LS and the remaining LS was dried at a ventilated place for 30 days to prepare a dried LS. Then, the obtained dried LS was ground into powder and filtered through a 200-mesh sieve.

2.3 Preparation of LS-CQDs

Two grams of dried LS powder and 50 mL of pure water were mixed and placed into the PTFE-lined hydrothermal synthesis reactor, followed by heating for 3 h at 180 °C. After the reaction, the obtained solution was filtered through a 0.45- μm polyether sulfone membrane. The filtrate was then centrifuged at 10,000 min^{-1} for 15 min and the supernatant was filtered again using a 0.22- μm syringe filter. The resulting filtrate was dialyzed for 2 days and the dialysis fluid was changed daily. After completing the dialysis, the solution was freeze-dried to obtain the desired solid LS-CQDs.

2.4 Determination of the fluorescence quantum yield (QY) and lifetime

The QY of LS-CQDs was measured with a standard procedure. Quinoline sulfate (QS) with 55 % QY was employed as the reference standard. The integrated fluorescence intensity and absorbance (A) values of LS-CQDs and QS solution were determined at the same excitation wavelength and the percentage of QY were calculated in accordance with Equation (1):

$$QY_{\text{CQD}} = QY_{\text{QS}} \cdot \frac{I_{\text{CQD}}}{I_{\text{QS}}} \cdot \frac{A_{\text{QS}}}{A_{\text{CQD}}} \cdot \left(\frac{n_{\text{CQD}}}{n_{\text{QS}}} \right)^2 \cdot 100 \% \quad (1)$$

where QY represents the fluorescence quantum yield (%), I refers to the integrated fluorescent intensity, A indicates the absorbance value and n stands for the refractive index of the solvent.

To determine the fluorescence lifetime of LS-CQDs, Equation (2) was used for the exponential-decay-curve fitting:²²

$$I_t = \sum_1^n A_n \cdot e^{-\frac{t}{\tau_n}} \quad (2)$$

where I represents the fluorescence intensity, A stands for the weight coefficient and τ represents the fluorescence lifetime.

Determination of Fe(III) ions with LS-CQDs

Solid LS-CQDs were dissolved and diluted to a 1 mg/L solution with ultrapure water. For the determination of Fe(III) ions, 2 mL of different concentrations of the Fe(III) ion solution were mixed with a CQD solution (ratio = 1:1, v/v). After a thorough mixing, the fluorescence intensity of the LS-CQDs solution was determined.

3 RESULTS

3.1 Morphological characterization

As illustrated in **Figure 1a**, the morphology of LS-CQDs exhibited a spherical shape with a uniform dispersion, which confirmed a successful preparation of LS-CQDs.²³ **Figure 1b** demonstrates the crystal lattices

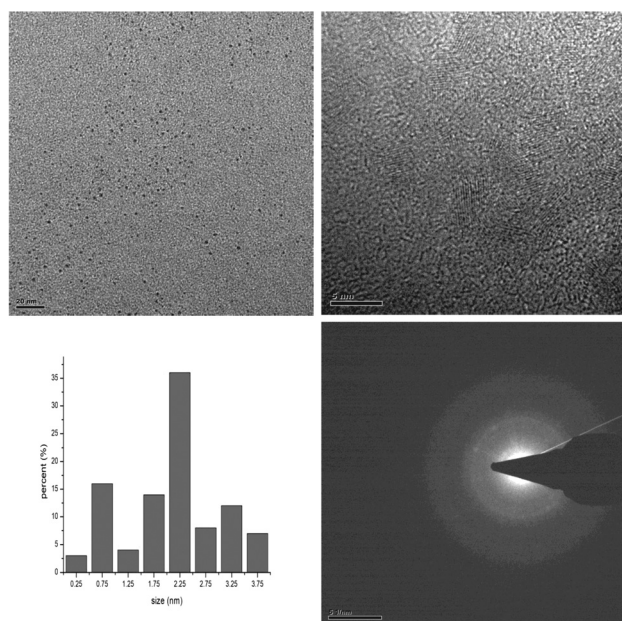


Figure 1: a) TEM image, b) high-resolution TEM image, c) particle-size distribution, d) SAED pattern of LS-CQDs

of LS-CQDs (lattice spacing = 0.22 nm), which are slightly smaller than those of the CQDs reported in other studies.^{24,25} **Figure 1c** indicates that the average particle size of LS-CQDs is 2.1 nm (ranging from 0.5 nm to 4 nm). **Figure 1d** reveals the selected-area electron-dif-

fraction (SAED) pattern of LS-CQDs, indicating the amorphous phase of LS-CQDs.²⁶

Photoluminescence and spectroscopic characterization

Figure 2a indicates the UV-visible spectrum of LS-CQDs. The existence of the maximum absorption peak at around 204 nm is due to the $\pi-\pi^*$ transition of the aromatic C=O bond.²⁷ In the inset, the LS-CQD solution is brown under the visible-light illumination, while emitting bright green under the UV-light illumination.

Figure 2b indicates the fluorescence emission and excitation of LS-CQDs. The maximum adsorption peak of the fluorescence intensity was located at 360 nm in the excitation spectra. **Figure 2c** indicates the excitation-dependent property of LS-CQDs, suggesting the occurrence of a redshift with the increasing excitation wavelengths. The PL is generated from a pre-existing surface defect on LS-CQDs, playing a major role in trapping the excitation energy and emitting light at a particular excitation wavelength, thus leading to an excitation-dependent property.

As shown in **Figure 2d**, different fluorescence-life-time values were observed and an average fluorescence-decay lifetime of 5.50 ns was determined. The quantum yield of LS-CQDs was calculated to be 1.9 %, which is relatively low compared to the CQDs synthesized from other carbon sources.^{28,29}

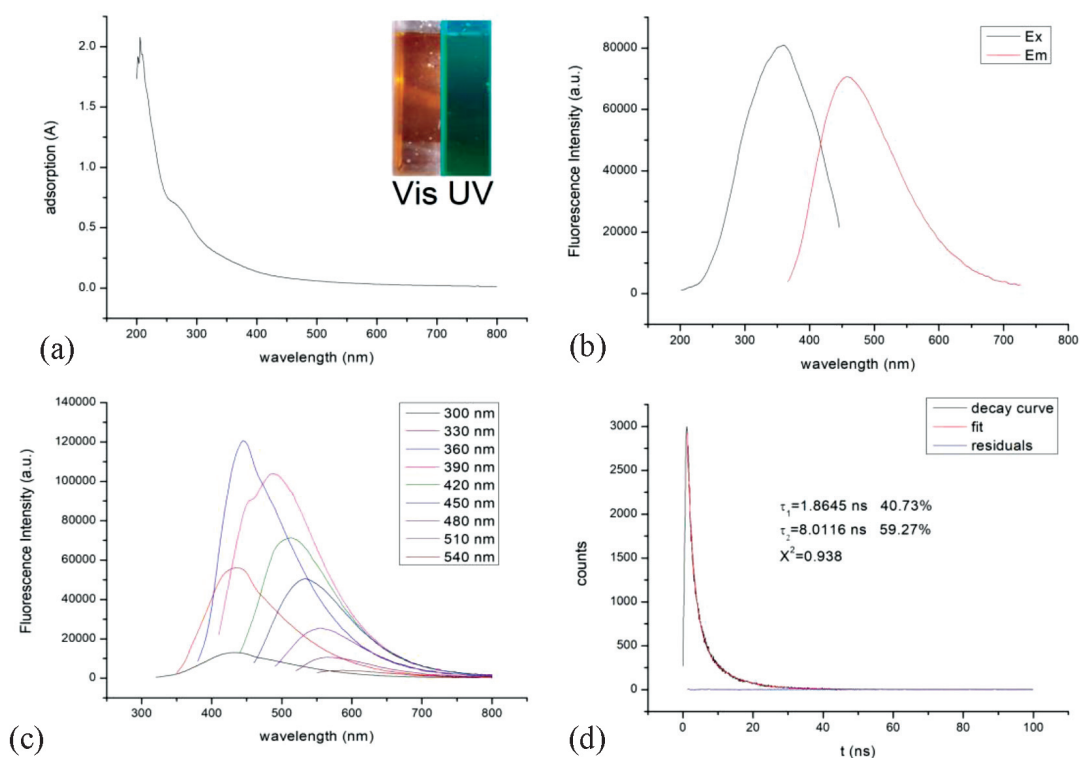


Figure 2: a) UV-visible spectrum (inset: photographs of LS-CQD solution under visible light (left) and UV light (right)), b) fluorescence emission and excitation spectra of LS-CQDs, c) emission spectra of LS-CQDs at excitation wavelengths varying from 300 nm to 540 nm, d) fluorescence-decay lifetime of LS-CQDs at a 360-nm excitation wavelength

3.2 Surface function group and structure characterization

The functional groups on the surfaces of LS-CQDs were characterized with an FTIR analysis. As shown in **Figure 3a**, a broad peak was observed at 3388 cm^{-1} , which corresponded to the -OH stretching vibration peak.³⁰ The peak at 2931 cm^{-1} was ascribed to the symmetric -C-H stretching vibration group, while the peaks at 1633 cm^{-1} and 1410 cm^{-1} were attributed to the presence of a -COO group. The peaks at 1256 cm^{-1} and 1048 cm^{-1} were corresponded to C-O-C and -C-N stretching vibration groups, respectively. The peak at 611 cm^{-1} was ascribed to the C-C stretching vibration group.

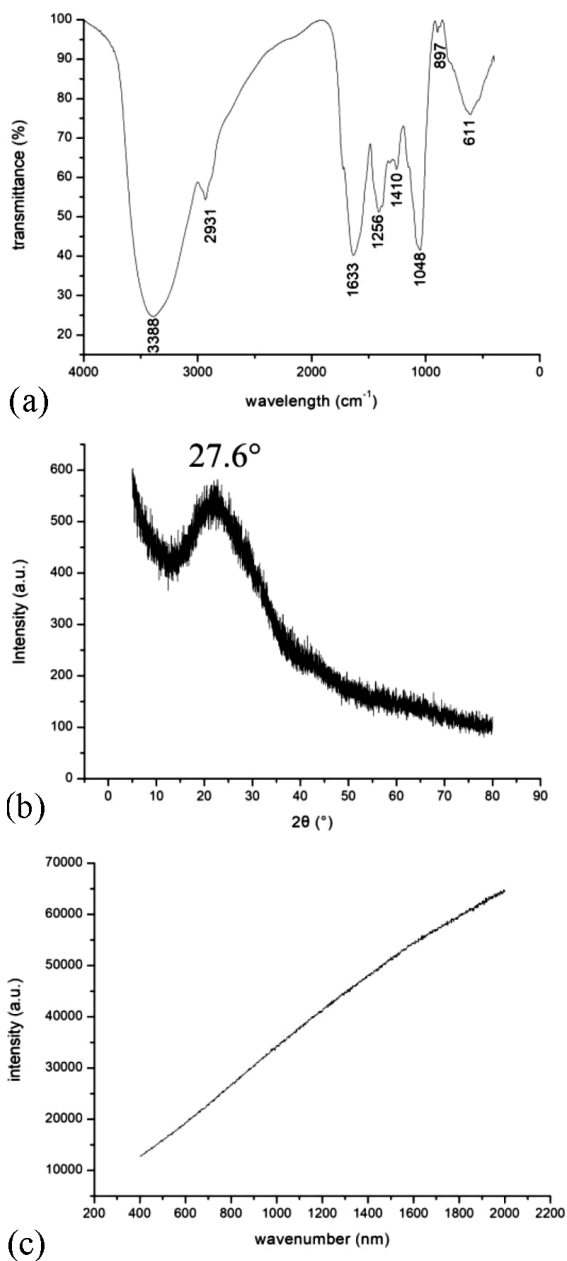


Figure 3: a) FTIR, b) XRD and c) Raman spectra of LS-CQDs

Figure 3b indicates the XRD pattern of LS-CQDs. There is an obvious absorption peak at around 27.6° , which demonstrates the amorphous form of LS-CQDs. This result is similar to a previous study.³¹

Figure 3c indicates the Raman spectrum of LS-CQDs. Typically, the fluorescence intensities of the D and G peaks in the Raman spectrum were used to calculate the graphitization degrees of LS-CQDs. As shown in **Figure 3c**, both the G peak (representing crystallinity) and D peak (representing the degree of disorder) are statistically insignificant. It is deduced that the fluorescence interference from LS-CQDs may impede the Raman-spectrum signal.^{32,33}

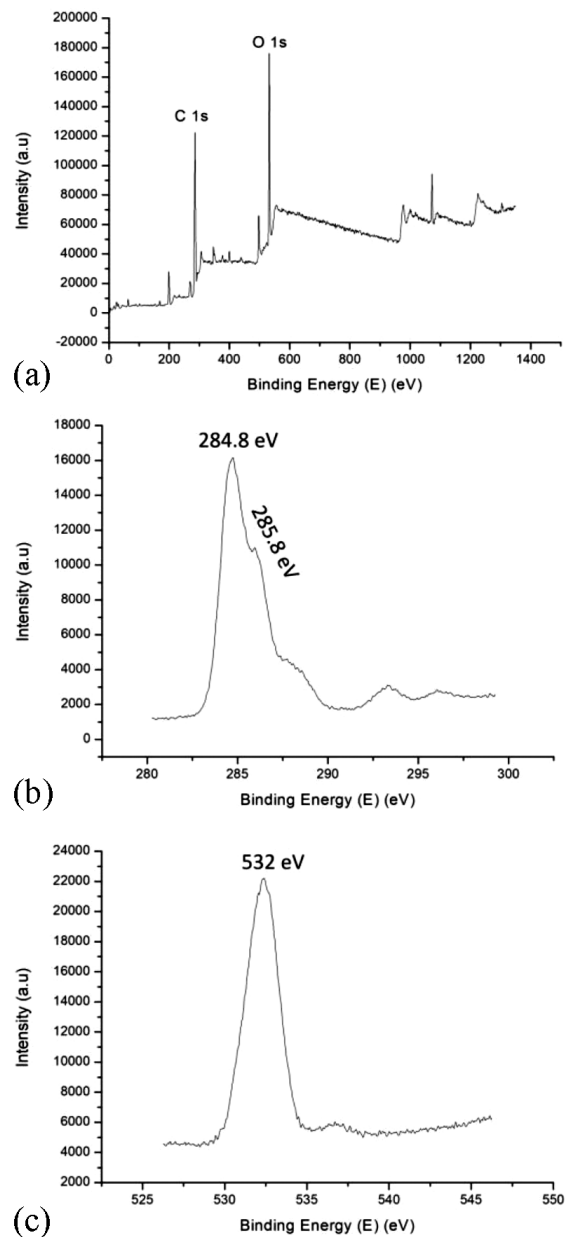
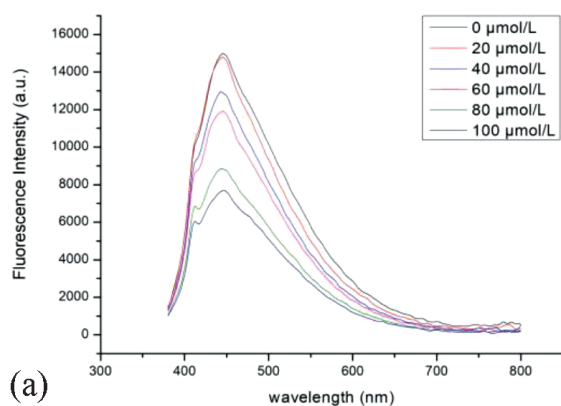


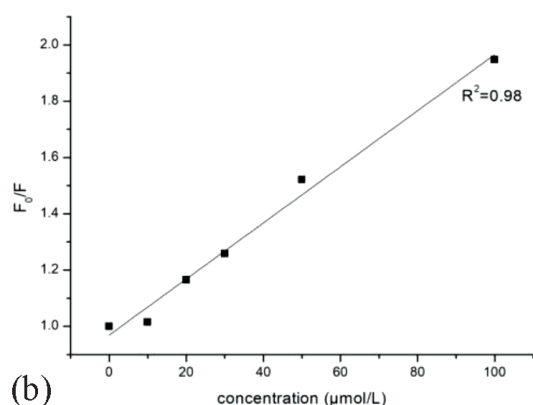
Figure 4: XPS spectra of LS-CQDs: a) XPS survey spectrum and binding-energy spectra of b) C1s and c) O1s

3.3 XPS analysis

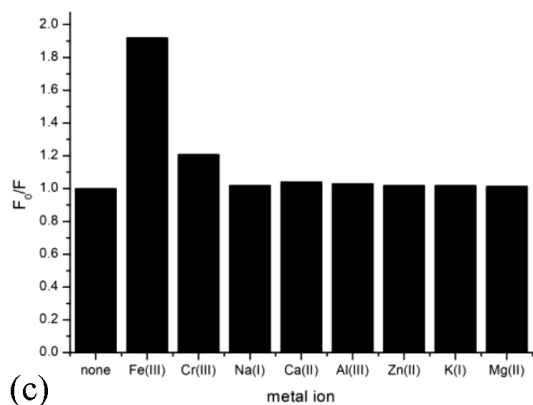
X-ray photoelectron spectroscopy was employed to assess the surface composition and oxidation state of LS-CQDs. **Figure 4a** shows an XPS survey spectrum with two obvious shoulder peaks at 285 eV and 532 eV, which correspond to the characteristic peaks of C1s and O1s, respectively. **Figure 4b** indicates the high-resolution spectrum of C1s with a major peak at 284.8 eV and a weak peak at 285.8 eV, which correspond with the C-C and C-N bond formation on sp^2 carbon, respectively.³⁴ **Figure 4c** indicates the high-resolution spectrum of O1s with a shoulder peak at 532 eV, which is ascribed to the



(a)



(b)



(c)

Figure 5: a) Emission spectra of different concentrations of Fe(III) ions, b) the standard curve of F_0/F at a 360 nm excitation wavelength, c) the quenching efficiency (F_0/F) of other metal ions against Fe(III) ions

C-OH/C-O-C groups.³⁵ The XPS results demonstrate the presence of a water-soluble oxygen-containing function group on the surface of LS-CQDs.

3.4 Detection of Fe(III) ions

Figure 5a displays the emission spectra of LS-CQDs with Fe(III) concentrations varying from 0 $\mu\text{mol/L}$ to 100 $\mu\text{mol/L}$. An obviously decreased fluorescence intensity at a peak of 449 nm was observed, indicating the fluorescence-quenching effect of Fe(III) on LS-CQDs.

Figure 5b shows a calibration graph of F_0/F versus Fe(III) concentrations where F_0 and F are the fluorescence intensities of LS-CQDs at 449 nm without and with varying Fe(III) concentrations, respectively. An R^2 value of 0.98 was obtained, suggesting a positive correlation between the F_0/F of LS-CQDs and the concentrations of Fe(III). In addition, the results also show the suitability of LS-CQDs for the determination of Fe(III) ions.

Figure 5c shows the fluorescence quenching efficiency (F_0/F) of the other metal ions (i.e., Al^{3+} , Ca^{2+} , Cr^{3+} , K^+ , Mg^{2+} , Na^+ and Zn^{2+}) on LS-CQDs at the same concentration (100 $\mu\text{mol/L}$). Except for Cr(III), all the metal ions exhibited no obvious effect on the fluorescence intensity of LS-CQDs, confirming the high selectivity of LS-CQDs for the Fe(III) ion detection.

In this study, no remarkable shift occurs at the emission peak around the center at 449 nm, indicating that the fluorescence-quenching mechanism should probably be attributed to electron transfer.³⁶ Further, the kinetic mechanisms of the fluorescence-quenching effect were elucidated.

Typically, fluorescence quenching can be classified with regard to the static and/or dynamic quenching effects. The ground-state complex formation model of the static or dynamic quenching effect was determined in accordance with the Stern-Volmer relationship Equation (3):

$$F_0/F = 1 + K_{SV}C_q = 1 + K_q\tau_0 C_q \quad (3)$$

where K_{SV} stands for the quenching constant; τ_0 represents the average lifetime of LS-CQDs (5.5 ns); and K_q refers to the quenching-rate constant. Notably, K_q was determined to be $4.27 \times 10^{11} \text{ M}^{-1} \text{ s}^{-1}$, which is markedly greater than the maximum scatter collision quenching constant ($\sim 1.0 \times 10^{10} \text{ M}^{-1} \text{ s}^{-1}$). These results indicate the static quenching effect of Fe(III) on LS-CQDs.

4 CONCLUSIONS

CQDs were prepared with a hydrothermal synthesis using LS as the carbon source. The synthesized LS-CQDs exhibited a uniform particle-size distribution (the mean = 2.1 nm) and were slightly smaller than the previously reported CQDs. The synthesized LS-CQDs demonstrated wavelength-dependent excitation and emitted a green light at 365 nm. In addition, LS-CQDs were

employed as a fluorescent probe for the Fe(III) ion detection. With the increasing Fe(III) ion concentration, the fluorescence quenching rate of LS-CQDs on Fe(III) ions was increased. However, the synthesized LS-CQDs still possess the disadvantage of a low QY, which should be improved in future studies.

Acknowledgment

The authors sincerely thank for the funding from Study on Comprehensive Control of Rocky Desertification and Ecological Service Function Improvement in Karst Peaks (No. 2016YFC0502402).

5 REFERENCES

- A. K. Das, A. Marwal, V Pareek, Y Joshi, Surface Engineering of Magnetite Nanoparticles by Plant Protein: Investigation into Magnetic Properties, Nano Hybrids & Composites, 11 (2016), 38–44, doi:10.4028/www.scientific.net/NHC.11.38
- P. N Dube, A. Shwetha, B. B Hosetti, Impact of copper cyanide on the key metabolic enzymes of freshwater fish *Catla catla* (Hamilton), Biotechnology in Animal Husbandry, 30 (2014) 3, 499–508, doi:10.2298/BAH1403499D
- V. Mitrovic, A. F. Hernandez, M. Meyer, Role of guanylate cyclase modulators in decompensated heart failure, Heart Fail. Rev., 14 (2009) 4, 309–316, doi:10.1007/s10741-009-9149-7
- D. S. Kalinowski, D. R. Richardson, Future of toxicology—iron chelators and differing modes of action and toxicity: the changing face of iron chelation therapy, Chem. Res. Toxicol., 20 (2007) 5, 715–724, doi:10.1021/tx700039c
- H. Li, K. Tsay, H. Wang, J. Shen, S. Wu, J. Zhang, N. Jia, S. Wessel, Durability of PEM fuel cell cathode in the presence of Fe³⁺ and Al³⁺, J. Power Sources, 195 (2010) 24, 8089–8093, doi:10.1016/j.jpowsour.2010.07.003
- D. Liu, L. Ma, Target transformation factor analysis for simultaneous determination of Fe³⁺ and Al³⁺ in rare earth samples, Spectroscopy & Spectral Analysis, 21 (2001) 3, 353–359, doi:10.1016/S1386-1425(01)00435-8
- D. Song, E. Ma, Z. Sun, H. Zhang, A layer-structured Eu-MOF as a highly selective fluorescent probe for Fe³⁺ detection through a cation-exchange approach, J. Mater. Chem., 22 (2012) 33, 16920–16926, doi:10.1039/c2jm32661b
- P. Qi, D. Zhang, Y. Wan, Morphology-tunable polydopamine nanoparticles and their application in Fe³⁺ detection, Talanta, 170 (2017), 173–179, doi:10.1016/j.talanta.2017.03.093
- R. Zhu, T. Wang, D. Wang, Zinc-based CPs for effective detection of Fe³⁺ and Cr^{2O7}-ions, New J. Chem., 43 (2019) 3, 1494–1504, doi:10.1039/C8NJ05508D
- S. Chaudhary, M. D. Milton, Dicationic imidazolium salts as fluorescent probes for selective detection of Fe³⁺ ion in pure aqueous media, J. Photochem. Photobiol. A: Chem., 356 (2018), 595–602 doi:10.1016/j.jphotochem.2018.02.003
- W. Wang, N. Gong, H. Yin, Two Stable Terbium–Organic Frameworks Based on Pre-designed Functionalized Ligands: Selective Sensing of Fe³⁺ Ions and C₂H₂/CH₄ Separation, Inorg. Chem., 58 (2019) 15, 10295–10303, doi:10.1021/acs.inorgchem.9b01465
- J. Chen, X. Jiang, C. Zhang, Reversible Reaction-Based Fluorescent Probe for Real-Time Imaging of Glutathione Dynamics in Mitochondria, Acs Sensors, 2 (2017) 9, 1257–1261, doi:10.1021/acssensors.7b00425
- G. Jiang, G. Zeng, W. Zhu, A selective and light-up fluorescent probe for -galactosidase activity detection and imaging in living cells based on an AIE tetraphenylethylene derivative, Chem. Commun., 53 (2017) 32, 4505–4508, doi:10.1039/C7CC00249A
- V. K. Singh, V. Singh, P. K. Yadav, Bright-blue-emission nitrogen and phosphorus-doped carbon quantum dots as a promising nanoprobe for detection of Cr(vi) and ascorbic acid in pure aqueous solution and in living cells, New J. Chem., 42 (2018) 15, 12990–12997, doi:10.1039/C8NJ02126K
- V. K. Singh, V. Singh, P. K. Yadav, S. Chandra, Nitrogen doped fluorescent carbon quantum dots for on-off-on detection of Hg²⁺ and glutathione in aqueous medium: Live cell imaging and IMPLICATION logic gate operation, J. Photochem. Photobiol. A: Chem., 384 (2019), 112042, doi:10.1016/j.jphotochem.2019.112042
- Y. Fu, S. Wu, H. Zhou, Carbon Dots and a CdTe Quantum Dot Hybrid-Based Luorometric Probe for Spermine Detection, Ind. Eng. Chem. Res., 59 (2020) 4, 1723–1729, doi:10.1021/acs.iecr.9b06289
- J. Yue, L. Li, L. Cao, Two-Step Hydrothermal Preparation of Carbon Dots for Calcium Ion Detection, ACS Applied Materials & Interfaces, 11 (2019) 47, 44566–44572, doi:10.1021/acsami.9b13737
- Z. Zhang, D. Zhang, C. Shi, 3,4-Hydroxypyridinone-Modified Carbon Quantum Dot as a Highly Sensitive and Selective Fluorescent Probe for Rapid Detection of Uranyl Ions, Environmental Science: Nano, 6 (2019) 5, 1457–1465, doi:10.1039/C9EN00148D
- Y. Duan, H. Zhang, F. Xu, Inhibition effect of procyanidins from lotus seedpod on mouse B16 melanoma in vivo and in vitro, Food Chem., 122 (2010) 1, 84–91, doi:10.1016/j.foodchem.2010.02.020
- Q. He, H. Wang, J. Zhang, Lotus seedpod as a low-cost biomass for potential methylene blue adsorption, Water Science & Technology A Journal of the International Association on Water Pollution Research, 74 (2016) 11, 2560–2567, doi:10.2166/wst.2016.423
- D. Zang, R. Zhu, W. Zhang, Corrosion Resistance: Corrosion-Resistant Superhydrophobic Coatings on Mg Alloy Surfaces Inspired by Lotus Seedpod, Adv. Funct. Mater., 27 (2017) 8, 1605446, doi:10.1002/adfm.201770050
- D. Magde, R. Wong, P. G. Fluorescence Quantum Yields and Their Relation to Lifetimes of Rhodamine 6G and Fluorescein in Nine Solvents: Improved Absolute Standards for Quantum Yields, Photochem. Photobiol., 75 (2002) 4, 327–334, doi:10.1562/0031-8655(2002)0750327fqyatr2.0.Co2
- J. Hu, X. Bai, Y. Liu, Functionalized carbon quantum dots with dopamine for tyrosinase activity analysis, Anal. Chim. Acta, 995 (2017), 99–105, doi:10.1016/j.aca.2017.09.038
- X. Deng, Y. Feng, H. Li, Detection of Ferric Iron Based on Fluorescence Quenching Effect of N-doped Carbon Quantum Dots, Chinese Journal of Analytical Chemistry, 45 (2017) 10, 1497–1503, doi:10.11895/j.issn.0253-3820.170344
- Y. Zhao, Y. Zhang, X. Liu, Novel carbon quantum dots from egg yolk oil and their haemostatic effects, Sci. Rep., 7 (2017) 1, 4452–4458, doi:10.1038/s41598-017-04073-1
- S. Ahmadian, M. Salavat, D. Ghanbari, Hydrothermal green synthesis of magnetic Fe₃O₄-carbon dots by lemon and grape fruit extracts and as a photoluminescence sensor for detecting of E. coli bacteria, Spectrochimica Acta Part A Molecular & Biomolecular Spectroscopy, 203 (2018) 5, 481–493, doi:10.1016/j.saa.2018.06.021
- B. Luo, H. Yang, B. Zhou, Facile Synthesis of Luffa Sponge Activated Carbon Fiber Based Carbon Quantum Dots with Green Fluorescence and Their Application in Cr(VI) Determination, ACS Omega, 5 (2020) 10, 5540–5547, doi:10.1021/acsoomega.0c00195
- H. Ding, Y. Ji, J. Wei, Facile synthesis of red-emitting carbon dots from pulp-free lemon juice for bioimaging, Journal of Materials Chemistry B, 5 (2017) 26, 5272–5277, doi:10.1039/c7tb01130j
- Y. Dong, H. Pang, H. Yang, Carbon-Based Dots Co-doped with Nitrogen and Sulfur for High Quantum Yield and Excitation-Independent Emission, Angew. Chem. Int. Ed., 52 (2013) 30, 7800–7804, doi:10.1002/anie.201301114
- R. Singh, S. Kashayap, V. Singh, QPRTase modified N-doped carbon quantum dots: A fluorescent bioprobe for selective detection of

- neurotoxin quinolinic acid in human serum, *Biosens. Bioelectron.*, 101 (2018) 15, 103–109, doi:10.1016/j.bios.2017.10.017
- ³¹ A. Meng, Q. Xu, K. Zhao, A highly selective and sensitive "on-off-on" fluorescent probe for detecting Hg(II) based on Au/N-doped carbon quantum dots, *Sensors Actuators B: Chem.*, 255 (2018) 1, 657–665, doi:10.1016/j.snb.2017.08.028
- ³² G. Zhang, L. Hu, K. Zhu, Contribution of oligomer/carbon dots hybrid semiconductor nanoribbon to surface-enhanced Raman scattering property, *Applied Surface Science*, 364 (2016) 28, 660–669, doi:10.1016/j.apsusc.2015.12.214
- ³³ S. Zhu, Q. Meng, L. Wang, Highly Photoluminescent Carbon Dots for Multicolor Patterning, Sensors, and Bioimaging, *Angewandte Chemie International Edition*, 52 (2013) 14, 3953–3957, doi:10.1002/anie.201300519
- ³⁴ X. Teng, C. Ma, C. Ge, Green synthesis of nitrogen-doped carbon dots from konjac flour with "off-on" fluorescence by Fe³⁺ and l-lysine for bioimaging, *Journal of Materials Chemistry B*, 2 (2014) 29, 4631–4639, doi:10.1039/C4TB00368C
- ³⁵ W. Wang, Y. Lu, H. Huang, Facile synthesis of water-soluble and biocompatible fluorescent nitrogen-doped carbon dots for cell imaging, *Analyst*, 139 (2014) 7, 1692–1696, doi:10.1039/C3AN02098C
- ³⁶ H. Hamishehkar, B. Ghasemzadeh, A. Naseri, Carbon dots preparation as a fluorescent sensing platform for highly efficient detection of Fe(III) ions in biological systems, *Spectrochimica Acta Part A: Molecular and Biomolecular Spectroscopy*, 150 (2015), 934–939, doi:10.1016/j.saa.2015.06.061